DOI: 10.61782/fa.2025.0572

FORUM ACUSTICUM EURONOISE 2025

MODAL APPROACHES FOR MODELLING NONLINEAR ACOUSTICS IN 2D AXISYMMETRIC DOMAINS: APPLICATION TO BRASS INSTRUMENTS

Filipe Soares[1*] **Bruno Cochelin**[1] **Vincent Freour**[1,2]
Christophe Vergez[1] **Keita Arimoto**[2]

[1] Aix Marseille Univ, CNRS, Centrale Med, LMA UMR7031, Marseille, France
[2] Yamaha Corporation, Research and Development Division, 101 Nakazawa-cho, Naka-ku, Hamamatsu, Shizuoka 430-8650, Japan

ABSTRACT

The modelling approach presented here aims at developing accurate, yet computationally efficient, numerical models of brass instrument resonators including nonlinear propagation, viscothermal losses and 2D radiation effects. Firstly, we propose the use of the Blackstock equation to model the nonlinear acoustic propagation inside the resonator, a more appropriate choice when dealing with nonlinear standing wave patterns, compared to the commonly used Burger's equation. The initial step of the approach consists in obtaining a complex modal basis from a 2D-axisymmetric finite element model of the linearized equations. Here, we include a bounded domain outside the resonator with a nonreflecting boundary condition as well as the effect of viscothermal losses at the interior walls. The nonlinear Blackstock equation is then projected onto the resulting 2D complex modal basis, leading to a compact set of nonlinear ODEs. This leads to exploitable reduced formulations adapted to quick temporal simulations, bifurcation analysis or parametric studies, retaining nevertheless the accuracy of 2D models. The explicit account of the exterior acoustic field also allows for the calculation of radiated sound pressures as well as directivity patterns. Experimental validation and illustrative numerical results are presented for a simplified trumpet geometry in both linear and nonlinear scenarios.

Keywords: *nonlinear acoustic propagation, brass instruments, 2D axisymmetric modelling, complex modes*

[*] ***Corresponding author***: *filipedcsoares@gmail.com*

1. INTRODUCTION

The physical modelling of brass wind instruments has received considerable attention in the last few decades [1]. These instruments constitute complex physical systems that, from the point of view of physical modelling, still present many challenging aspects. Here our focus is on the modelling of the instrument itself, i.e. without the influence of the lip vibration and the associated control by the musician.

Widely used and relatively simple models (typically in 1D frameworks) are able to qualitatively reproduce measured behavior. However, simplified models often present inherent limitations that prevent them from capturing the more subtle features of real instruments. For example, 1D models often rely on the assumption of plane wave propagation which, albeit reasonable in the narrower parts of the instrument bore, clearly breaks down at the exit of the instrument. Another important aspect is related to nonlinear acoustic propagation inside the resonator, a particularly relevant feature influencing the timbre of brass instruments [2]. Although some numerical studies have dealt with this topic, they almost exclusively rely on the Burgers equation [3][4]. However, this equation assumes only forward or backward propagating waves and its use in the context of brass instruments is questionable since standing waves are formed inside the instrument.

In commercial contexts, where manufacturers are interested in optimizing/fine-tuning certain aspects of their instruments, the accuracy provided by these simplified models often falls short of the desired goals. The motivation behind this work lies on the need to build a physical model that provides: (1) an accurate description of the pertinent acoustic phenomena, including an appropriate nonlinear acoustic propagation model, viscothermal losses at the walls as well as 2D propagation and radiation effects and

(2) an efficient and exploitable framework (low computational cost) that can be used for quick temporal simulations, parametric studies, optimization, bifurcation analysis, etc. The approach proposed here aims to bridge the accuracy provided by 2D-axisymmetric models and the efficiency of reduced-order modal approaches. The general idea consists in using a 2D finite element (FE) model of the linearized equations to obtain a suitable modal basis that can then be used to project the nonlinear equations, leading to exploitable reduced-order models (composed of a set of nonlinear ODEs). Due to the localized nature of the involved energy dissipation mechanisms (viscothermal and radiation losses), the eigenvalue problem stemming from the linearized 2D FE model leads to a complex modal basis [5]. In this particular context, the full potential of modal decomposition is highlighted. Firstly, the modal basis serves to spatially discretize the problem. Secondly, because modes have characteristic natural frequencies, they also serve to "discretize" the system in the frequency domain, i.e. modes whose natural frequencies fall outside the frequency bands of interest can generally be neglected. Thirdly, modes have characteristic damping ratios which encapsulate, in a simple manner, the often-times intricate dissipation mechanisms. For example, viscothermal losses are notably difficult to model in the time-domain since they give rise to fractional-order derivatives [6]. These can however be easily represented in a modal framework, suited for both frequency and time domain analysis. Finally, modal approaches have also been proven useful to treat nonlinear terms in an efficient manner [7] as well as for mitigating numerical dispersion, a common problem when solving stiff wave equations using finite difference or finite elements methods in the time domain [8].

2. MODEL DESCRIPTION

2.1 Nonlinear acoustics in 3D domains

In most applications, not involving explosions or other supersonic events, nonlinear acoustics are typically modelled through what are called weakly-nonlinear models. Starting from the set of irrotational compressible Euler equations and a state equation for the fluid, a wide variety of models have been proposed over the years, well documented in an historical review by Jordan [9]. Of particular interest to us, are the so-called wave equations, where the acoustic field is represented by a single scalar variable. In this work we propose the use of the Blackstock equation, written here in terms of the velocity potential $\phi(t, \mathbf{x})$

$$\ddot{\phi} - c^2\Delta\phi + 2(\nabla\dot{\phi})(\nabla\phi) + (\gamma-1)\dot{\phi}(\Delta\phi) = 0 \qquad (1)$$

where the over-dot denotes temporal derivatives, ∇ and Δ are the gradient and Laplacian operators, c is the speed of sound in the fluid and γ its adiabatic index. This second-order approximation of the more general Söderholm formulation is bound to be valid for acoustic Mach numbers up to $M < 0.1$. Note that this equation is equivalent to the more commonly used Kuznetsov equation [10].

Assuming the curved bents in typical brass instruments are acoustically negligible, Eq.(1) can be written in axisymmetric cylindrical coordinates (r, z) as

$$\begin{aligned}\ddot{\phi} - c^2\left[\frac{1}{r}\frac{\partial}{\partial r}\left(r\frac{\partial\phi}{\partial r}\right) + \frac{\partial^2\phi}{\partial z^2}\right] \cdots \\ +2\left(\frac{\partial\dot{\phi}}{\partial r} + \frac{\partial\dot{\phi}}{\partial z}\right)\left(\frac{\partial\phi}{\partial r} + \frac{\partial\phi}{\partial z}\right) \cdots \\ +(\gamma-1)\dot{\phi}\left[\frac{1}{r}\frac{\partial}{\partial r}\left(r\frac{\partial\phi}{\partial r}\right) + \frac{\partial^2\phi}{\partial z^2}\right] = 0\end{aligned} \qquad (2)$$

Additionally, because of the larger cross-section at the exit of the instrument, acoustic levels are relatively weaker. Hence, large amplitude acoustic perturbations and nonlinear propagation are known to occur primarily at the narrower parts of the horn [2], where the plane wave assumption is reasonable. This leads us to the conclusions that, in the context of brass instruments, the nonlinear terms in Eq.(2) involving the radial derivative $\partial\phi/\partial r$ can confidently be neglected, leading to

$$\begin{aligned}\ddot{\phi} - c^2\left[\frac{1}{r}\frac{\partial}{\partial r}\left(r\frac{\partial\phi}{\partial r}\right) + \frac{\partial^2\phi}{\partial z^2}\right] \cdots \\ +2\left(\frac{\partial\dot{\phi}}{\partial z}\right)\left(\frac{\partial\phi}{\partial z}\right) + (\gamma-1)\dot{\phi}\left(\frac{\partial^2\phi}{\partial z^2}\right) = 0\end{aligned} \qquad (3)$$

where only two quadratic nonlinear terms subsist.

2.2 Finite element axisymmetric model

As mentioned before, our first aim is to use a finite element discretization of the *linearized* model in order to obtain a suitable modal basis, which will serve as a basis of functions on which to subsequently project the nonlinear Blackstock equation. With regards to the acoustic domain then, we have simply the Helmholtz equation (linear wave equation in frequency domain). But furthermore, we need to consider two important dissipative boundary conditions representing: (1) radiation of energy towards the free-field and (2) the viscothermal losses occurring at the inner walls of the instrument. Concerning the former, we consider an exterior spherical domain whose outer boundary will

contain a nonreflecting condition, aimed at simulating an anechoic environment, as illustrated in Figure 1. For the viscothermal losses we have used the model proposed by Berggren et al. [11], which is based on the fact that, in air, viscothermal acoustic boundary layers (where losses take place) tend to be very small compared to reference dimensions/wavelengths and can hence be accurately approximated via an impedance boundary condition.

The complete linearized axisymmetric problem to be solved can then be written in the frequency domain as

$$\begin{aligned} k^2\phi - c_0^2\left[\frac{1}{r}\frac{\partial}{\partial r}\left(r\frac{\partial\phi}{\partial r}\right)+\frac{\partial^2\phi}{\partial z^2}\right] &= 0 \text{ in } \Omega \\ \left(\frac{1}{R}-ik\right)\phi+\frac{\partial\phi}{\partial n} &= 0 \text{ on } \Gamma_r \\ -\delta_v\frac{i-1}{2}\Delta\phi+\delta_t k^2\frac{(i-1)(\gamma-1)}{2}\phi+\frac{\partial\phi}{\partial n} &= 0 \text{ on } \Gamma_{vt} \\ \frac{\partial\phi}{\partial n} &= 0 \text{ on } \Gamma_w \end{aligned} \tag{4}$$

where the acoustic boundary layer lengths are given by

$$\delta_v=\sqrt{\frac{2\nu}{\omega}}\ , \quad \delta_t=\sqrt{\frac{2\kappa}{\omega\rho C_p}} \tag{5}$$

with ρ the fluid static density, ν its kinematic viscosity, κ its thermal conductivity and C_p the coefficient of specific heat at constant pressure.

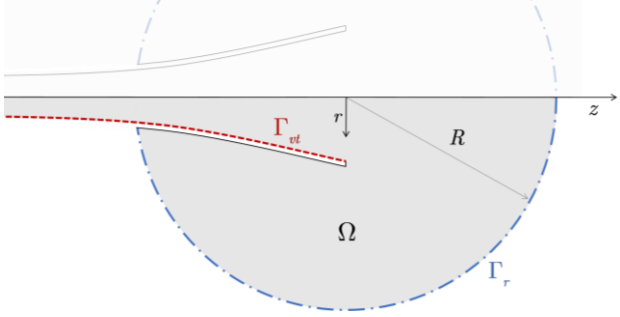

Figure 1. Diagram of the considered axisymmetric model. The dashed and dash-dotted lines correspond to the viscothermal Γ_{vt} and radiative Γ_r boundaries, respectively.

It is worth noting that the problem is here formulated in terms of acoustic velocity potential $\phi(r,z)$, but an equivalent formulation for the acoustic pressure can be obtained by replacing directly $\phi(r,z)$ by $p(r,z)$.

For compactness, we do not derive here the weak formulation or the FE discretization procedures, as these can be found in reference literature [12]. We simply note that second-order (6-node) triangular elements were used and the maximal size of each element $h_{\max}$ was set to at least one-fifth of the smallest considered wavelength.

2.3 Complex modal decomposition

After the FE spatial discretization, we obtain a dynamical system in the following form

$$\mathbf{M}\ddot{\boldsymbol{\phi}}(t)+\mathbf{C}\dot{\boldsymbol{\phi}}(t)+\mathbf{K}\boldsymbol{\phi}(t)=\mathbf{f}(t) \tag{6}$$

where $\boldsymbol{\phi}$ is a column vector of the velocity potential located at nodes of the FE discretized field and $\mathbf{f}(t)$ is a generic force vector that can represent external and/or nonlinear forces. Because of the localized nature of the modeled dissipative phenomena (radiation and viscothermal losses), our system belongs to a class of problems said to have non-classical damping. In practice, this prevents us from using typical modal approaches based on the real-valued modes shapes ($\mathbf{w}$), as these are not able to decouple the damped equations of motion. Here, we need to resort to complex modal analysis which is based around the state-space version of Eq.(6), arrived at by defining $\boldsymbol{\alpha}(t)=\dot{\boldsymbol{\phi}}(t)$, leading to

$$\mathbf{A}\dot{\mathbf{z}}(t)+\mathbf{B}\mathbf{z}(t)=\mathbf{F}(t) \tag{7}$$

with

$$\mathbf{A}=\begin{bmatrix}\mathbf{C} & \mathbf{M}\\ \mathbf{M} & 0\end{bmatrix}\ ;\ \mathbf{B}=\begin{bmatrix}\mathbf{K} & 0\\ 0 & -\mathbf{M}\end{bmatrix}\ ;\ \mathbf{z}(t)=\begin{Bmatrix}\boldsymbol{\phi}(t)\\ \boldsymbol{\alpha}(t)\end{Bmatrix}\ ;\ \mathbf{F}(t)=\begin{Bmatrix}\mathbf{f}(t)\\ 0\end{Bmatrix} \tag{8}$$

Solving the associated eigenvalue problem

$$(\lambda\mathbf{A}+\mathbf{B})\mathbf{u}=\mathbf{0} \tag{9}$$

leads us to the complex eigenvalues $\lambda_n\in\mathbb{C}$ and complex eigenvectors $\mathbf{u}_n\in\mathbb{C}$. Since $\mathbf{A}$ and $\mathbf{B}$ are symmetric, eigensolutions occur in pairs of complex conjugates

$$(\lambda_n,\ \bar{\lambda}_n)\ ;\ (\mathbf{u}_n,\bar{\mathbf{u}}_n)=\begin{Bmatrix}\mathbf{v}_n\\ \lambda_n\mathbf{v}_n\end{Bmatrix},\begin{Bmatrix}\bar{\mathbf{v}}_n\\ \bar{\lambda}_n\bar{\mathbf{v}}_n\end{Bmatrix} \tag{10}$$

where the overbar denotes complex conjugation. The full modal matrix of the first-order system is then

$$\hat{\mathbf{U}}=\begin{bmatrix}\mathbf{V} & \bar{\mathbf{V}}\\ \mathbf{V}\boldsymbol{\Lambda} & \bar{\mathbf{V}}\bar{\boldsymbol{\Lambda}}\end{bmatrix} \text{ with } \begin{cases}\mathbf{V}=\begin{bmatrix}\mathbf{v}_1,\dots\ \mathbf{v}_N\end{bmatrix}\\ \boldsymbol{\Lambda}=\text{diag}\ \lambda_1,\dots\ \lambda_N\end{cases} \tag{11}$$

Then, the complex modal transformation can be written in the following forms, due to its conjugate symmetry

$$\mathbf{z}(t)=\sum_{n=1}^{N}[\mathbf{u}_n q_n(t)+\bar{\mathbf{u}}_n\bar{q}_n(t)]=\mathbf{U}\mathbf{q}(t)+\bar{\mathbf{U}}\bar{\mathbf{q}}(t) \tag{12}$$

where $\mathbf{q}(t)$ are the modal coordinates and $\mathbf{U} = [\mathbf{V}\ \mathbf{V\Lambda}]^T$ is the reduced modal matrix of size $2N \times N$ pertaining to only one side of the conjugate pairs. Finally, replacing Eq.(12) in Eq.(7) and pre-multiplying by $\mathbf{U}^T$ leads to the reduced decoupled system

$$\dot{\mathbf{q}}(t) + \mathbf{\Lambda q}(t) = \mathbf{V}^T\mathbf{f}(t) \tag{13}$$

which is of size N (using only one mode of each conjugate pair), first-order in time and where coefficients and variables are complex-valued.

2.4 Projection of external forces and nonlinear terms

Since we can obtain an (approximate) continuous representation of modes shapes $\mathbf{v}_n$ from the FE model, the same procedure can be performed in a continuous framework where associated integrations (modal projections) can be performed numerically using Gaussian quadrature. With that said, the generic force terms presented in Eq.(13) can also be represented in continuous form

$$\mathbf{v}_n^T\mathbf{f}(t) \quad \Leftrightarrow \quad \int_\Omega f(r,z,t)V_n(r,z)drdz \tag{14}$$

where $f(r,z,t)$ is a generic force term and $V_n(r,z)$ is the continuous version of the n-th complex mode shape. If we now consider an expanded force term composed of a generic external force as well as the nonlinear terms in Eq.(3), expanded in modal coordinates, we obtain

$$\begin{aligned} f(r,z,t) = {} & g_{\text{ext}}(t)S(r,z) \\ & - \sum_{k,m}^{2N} \left[2V_m'V_k' + (\gamma-1)V_mV_k''\right]\dot{q}_m(t)q_k(t) \end{aligned} \tag{15}$$

where, to simplify notation, we use the over-dash represent the partial derivative $\partial\,/\,\partial z$. Note that we considered here an external force with separable spatial and temporal components, i.e. $g_{\text{ext}}(t)S(r,z)$. Finally, replacing the expansion (15) into (13) yields the final set of N nonlinear complex-valued ODEs

$$\dot{q}_n(t) + \lambda_n q_n(t) = g_{\text{ext}}(t)S_n + \sum_{k,m}^{2N} A_{kmn}\dot{q}_m(t)q_k(t) \tag{16}$$

for $n = 1,2...N$, where the constant terms associated with the modal projection are given by

$$A_{kmn} = \int_\Omega \left[2V_m'V_k' + (\gamma-1)V_mV_k''\right]V_n drdz \tag{17}$$

$$S_n = \int_\Omega S(r,z)V_n(r,z)drdz \tag{18}$$

At this point, there are a few important aspects of the derived system (16) that should be underlined. Firstly, the nonlinear tensor A_{kmn} is constant and is calculated "off-line", i.e. prior to any temporal integrations, nonlinear analysis, etc. Secondly, note that even though the original equations have two distinct nonlinear terms, these have the same temporal character. Therefore, when expanded in modal coordinates, they can be combined in a single nonlinear tensor A_{kmn}. On the other hand, because we are using a complex modal basis (as opposed to real modes), nonlinear terms need to be calculated using both modes in each conjugate pair, leading to a complex tensor A_{kmn} of size $2N \times 2N \times N$. Thirdly, by choosing an appropriate truncation N, we can build reduced models that are tailored to specific applications, e.g. large N (say 50-100) for strongly nonlinear scenarios or smaller N (say 10-20) for linear, or weakly-nonlinear ones.

2.5 Illustrative results: complex modes of a trumpet with simplified geometry

Complex mode shapes are awkward to illustrate in a static image. This is because, contrary to the motion of real modes where all points move in unison, complex modes contain phase shifts between different spatial regions. Hence, while real modes represent standing wave patterns, complex modes are a combination of standing and travelling waves. They are generally represented by their real $\text{Re}[V_n(r,z)]$ and imaginary $\text{Im}[V_n(r,z)]$ parts separately. Moreover, complex modes are defined up to a multiplicative complex factor. In this case, it is often useful to "rotate" the complex mode by an angle β (i.e. multiply by $e^{-i\beta}$) such that it maximizes its real part [13]. In this way, we can assess the "degree of complexity" of each mode by examining how large is its imaginary part. Examples of some complex mode shapes of a simplified trumpet model are shown in Figure 2. We note that lower order modes have a nearly null imaginary part, meaning that they represent almost perfect standing waves (i.e. real modes). Higher order modes however have much larger imaginary parts, representing their radiative character. That is, these modes reflect essentially waves travelling out of the horn towards the free-field.

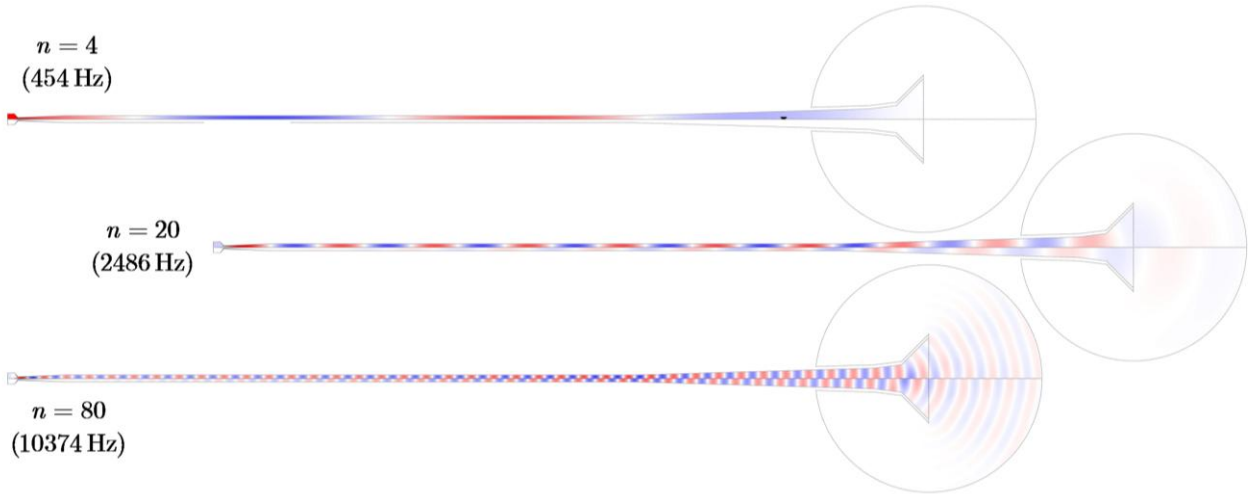

Figure 2. Some illustrative complex mode shapes $V_n(r, z)$ of the simplified trumpet. The real and imaginary parts are represented in the top and bottom of each plot, respectively. Note: modes shapes were rotated such that their real part is maximized (imaginary part minimized).

3. EXPERIMENTAL VALIDATION

To explore the effects of nonlinear propagation, an experimental set-up was prepared to excite the trumpet prototype harmonically. Acoustic excitation was provided by a BMS 4599 compression chamber placed at the entrance of the experimental prototype (without embouchure – i.e. only the cylindrical section plus the flaring horn section). Note however that this sort of set-up will inevitably influence the studied resonator since these drivers have an internal volume that is non-negligible. This volume was taken into account in the model, for validation purposes. However, naturally, the studied system in this case is not the same as that described in the previous section. The modal frequencies of the system were first identified via the exponential sine-sweep method. Subsequently, the system was excited at various modal frequencies at different amplitudes. A pressure sensor (Endevco 8507C-5) was placed iteratively on 40 locations along the resonator's length aimed at giving a spatial illustration of the nonlinear standing wave patterns. A second reference pressure sensor was fixed inside the cavity of the compression chamber to get a phase reference. The spatial distribution of the pressure inside the resonator when excited at the frequency of mode $n = 3$ (503 Hz) at different excitation amplitudes is shown in Figure 4. Analogous results from the model, obtained through temporal integrations using 100 complex modes are shown in Figure 5. Comparison of the experimental and modelled results are very satisfactory, with the model correctly representing the trends of the distorted standing wave patterns observed experimentally. Not only qualitatively, but also quantitatively, as the appearance and "level of distortion" appear to be congruent for the same values of the acoustic pressure. In a future work, different aspects of these results will be analyzed more thoroughly, as there are many more subtle aspects to be discussed.

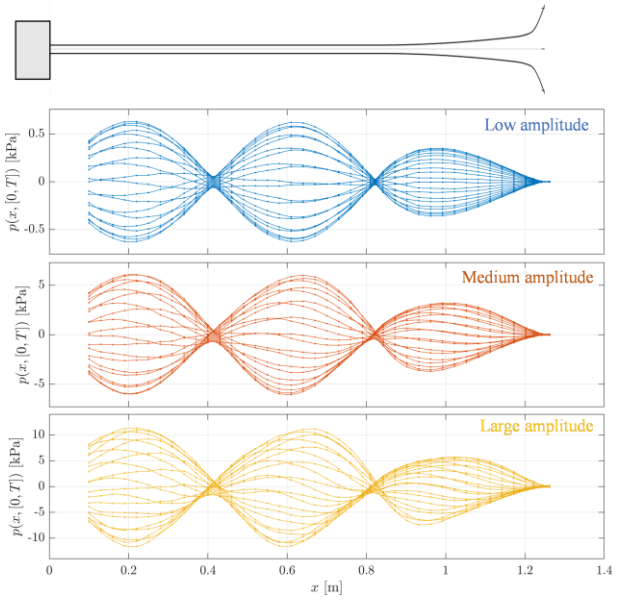

Figure 4. Experimental results: Snapshots of the measured pressure fields inside the trumpet at different amplitudes. Dots denotes the actual measurements while connecting lines were interpolated.

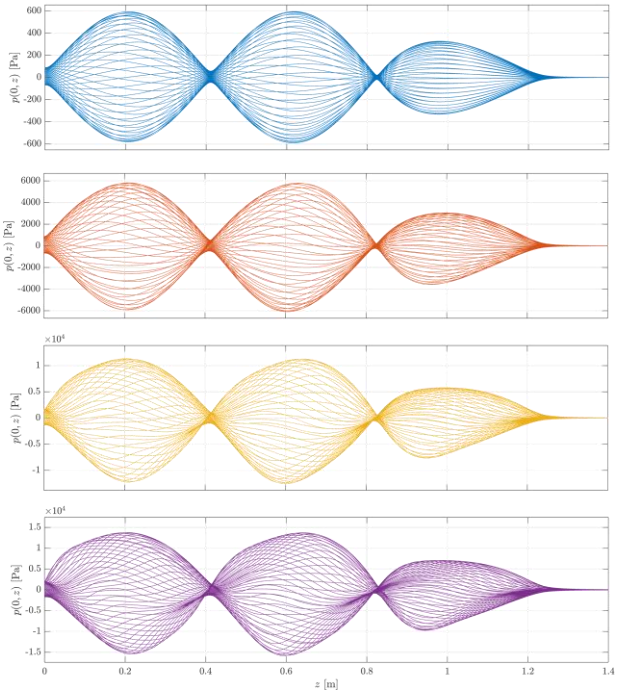

Figure 5. Modelling results: Snapshots of the modelled on-axis (r = 0) pressure fields inside the trumpet, excited harmonically at different amplitudes.

4. CONCLUSIONS

In this work we have shown how refined models of brass instruments, in a 2D axisymmetric framework, can be used to efficiently predict the behavior of real instruments, including a variety of complex physical phenomena like viscothermal losses at the walls, 2D radiation effects as well as nonlinear acoustic propagation. Within a reduced-order modal framework, these refined models convey essentially the same computational costs as the more typical 1D models used widely in the field. Moreover, the use of complex modes enables one to encapsulate intricate dissipative phenomena, like localized radiation or thermoviscous losses, in each modal component. This allows one to easily treat the problem in both the frequency and time domain, be that through temporal integrations, harmonic balance, numerical continuation, etc. The use of the Blackstock nonlinear acoustics equation instead of the more common Burger's equation allows us to calculate nonlinear standing wave patterns that can eventually be used to characterize brass instruments in terms of their capacity to produced "brassy" sounds. It is hoped that the developments shown here can stimulate a transition from descriptive towards predictive models of brass instruments.

5. REFERENCES

[1] A. Myers, J. Gilbert and M. Campbell, The Science of Brass Instruments, Springer, 2021.

[2] A. Myers, R. Pyle, J. Gilbert, M. Campbell, J. Chick and S. Logie, "Effects of nonlinear sound propagation on the characteristic timbres of brass instruments," *Journal of the Acoustical Society of America*, vol. 131, no. 1, pp. 678-688, 2012.

[3] S. Maugeais and J. Gilbert, "Nonlinear acoustic propagation applied to brassiness studies, a new simulation tool in the time domain," *Acta Acustica*, 2017.

[4] H. Berjamin, B. Lombart, C. Vergez and E. Cottanceau, "Time-domain numerical modeling of brass instruments including nonlinear wave propagation, viscothermal losses and lip vibration," *Acta Acustica united with Acustica*, vol. 103, no. 2, pp. 117-131, 2017.

[5] S. Krenk, "Complex modes and frequencies in damped structural vibrations," *Journal of Sound and Vibration*, pp. 981-996, 2004.

[6] N. Sugimoto, "Burgers equation with a fractional derivative: hereditary effects on nonlinear acoustic waves," *Journal of Fluid Mechanics*, vol. 225, no. 1, pp. 631-653, 1991.

[7] M. Ducceschi and C. Touzé, "Modal approach for nonlinear vibrations of damped impacted plates: Application to sound synthesis of gongs and cymbals," *Journal of Sound and Vibration*, vol. 344, pp. 313-331, 2015.

[8] C. Issanchou, S. Bilbao, J.-L. L. Carrou, C. Touzé and O. Doaré, "A modal-based approach to the nonlinear vibration of strings against a unilateral obstacle: Simulations and experiments in the pointwise case," *Journal of Sound and Vibration*, vol. 393, pp. 229-251, 2017.

[9] P. M. Jordan, "A survey of weakly-nonlinear acoustic models: 1910-2009," *Mechanics Research Communications*, vol. 73, pp. 127-139, 2016.

[10] B. Kaltenbacher and R. Brunnhuber, "Nonlinear Acoustics," Snapshots of modern mathematics from Oberwolfach , 2019.

[11] M. Berggren, A. Bernland and D. Noreland, "Acoustic boundary layers as boundary conditions," *Journal of Computational Physics*, vol. 371, pp. 633-650, 2018.

[12] L. Thompson, "A review of finite-element methods for time-harmonic acoustics," *Journal of the Acoustical Society of America*, vol. 119, no. 3, pp. 1315-1330, 2006.

[13] P. Vacher, B. Jacquier and A. Bucharles, "Extensions of the MAC criterion to complex modes," in *Proceedings of ISMA2010*, Leuven, Belgium, 2010.

[14] B. Cochelin, V. Freour and C. Vergez, "Exploiting the Use of Strong Nonlinearity in Dynamics and Acoustics: The Case of Musical Wind Instruments," in *Exploiting the Use of Strong Nonlinearity in Dynamics and Acoustics*, Springer Cham, 2024, pp. 121-149.